Integration of Landsat-8 and Reflectance Spectroscopy data for Mapping of Late Neoproterozoic Igneous Ring Complexes in an Arid Environment: a Case Study of Gebel El-Bakriyah Area, Eastern Desert, Egypt

Ahmed Abd El-Dayiem Abd El-Fatah[1*], Ahmed Ali Madani[1], Adel Abd Allah Surour[2], and Mokles Kamal Azer[3]

1. Department of Geology, Faculty of Science, Cairo University, Egypt
2. Department of Geological Sciences, Faculty of Science, Galala University, Egypt
3. Department of Geological Sciences, National Research Centre, Egypt

Article Info

Abstract

The present work aims to enhance the utilization of Landsat-8 data in geological mapping when they are paired with spectroscopic measurements and field observations. This is applied to map and differentiate the different plutonic rocks in the Gebel El-Bakriyah pluton, a peculiar igneous body in the central Eastern Desert of Egypt. Therefore, we use a combination of remote sensing techniques such as principal component analysis (PCA), band ratios, fusion technique, and spectroscopic measurements to interpret igneous lithologies, and produce a new geologic map of the Gebel El-Bakriyah area. A false-color composite principal component image PC1, PC2, and PC3 in red, green, and blue (RGB) discriminates between alkali feldspar granite, syenogranite, and younger gabbro. In general, the spectral profiles of granites exhibit three distinct absorption features in the 1.4, 1.9, and 2.2 μm wavelength regions. These features are attributed mainly to altered mineral products such as kaolinite, sericite, and chlorite. The spectral profiles of pink and alkali feldspar granites show a broad absorption feature at 0.9 μm, which is attributed to a considerable Fe content. The spectral profiles of fresh, younger gabbros exhibit absorption features around 1 μm and 2.2 μm. A false-color composite image provides the most accurate discrimination of the three varieties of younger granites with band ratios of 7/4, 6/3, and 3/1 in RGB. The data that appear in the present work strengthen the usefulness of Landsat-8 imagery and spectroscopic measurements as a prevailing grouping to discriminate and map Neoproterozoic shield rocks in the Eastern Desert of Egypt.

1. Introduction

Recently, remote sensing methods have offered helpful tools for earth sciences such as lithological discrimination and cartography, especially when updated maps are drafted. Accurate lithological connections are delineated and mapped using information from satellites with intermediate spatial and spectral resolution [1–10]. For example, the principal component analysis (PCA) and band ratio technique was applied by [11-15] to detect alteration zones, possibly gold bearing, in the Barramiya area along the transition between the central and Egypt's south-eastern deserts. In the southeastern desert, the Gebel Egat district's comprehensive mapping benefits from the integration of PCA, false-color composition (FCC), and band ratio technique of ASTER and Landsat ETM+ data, according to [16]. [17] stressed that using Landsat-8 images, PCA is a beneficial statistical method that offers the most accurate differentiation between various rock units. Recently [18,19], have discussed the usefulness of remote sensing for identifying the locations of alteration zones and gold mineralization in Egypt's Eastern Desert. Maps of significant structures such as shear zones and mega-thrusts in the Arabian-Nubian Shield are greatly aided by remote sensing techniques [20, 21]. The studied area, Gebel El-Bakriyah, shown

in Figure 1, is a small part of the southwestern part of Egypt's Eastern Central Desert that lies between longitudes 33° 41 ' to 33° 43 ' E and latitudes 25° 15' to 25° 17' N. According to [22], the area is covered by younger gabbro, a variety of granitoids (older and younger), in addition), and the Cretaceous sandstones of Nubian facies. They (op. cit.) produced a photogeological map of scale 1:10000 (Figure 2) that is still in use by most researchers concerned with the geology of the Gebel El-Bakriyah area. There is a significant need to update such a geological map with the help of modern remote sensing techniques to understand its geomorphology, structures, and natural resources. Here, we stress the importance

of alteration minerals in the spectral characteristics of lithologies such as the reflection of clay minerals, particularly kaolinite, and ferrous oxide. In the recent years, spectroscopic aspects such as infrared reflection can identify precise alterations in minerals [23]. Accordingly, different lithologies can be discriminated against [24–26]. Our work aims to recognize the plutonic rocks' spectral characteristics considering the impact of mineralogy, apply the acquired spectral knowledge to distinguish and outline the rock units using the processed Landsat-8 data, and produce a highly precise geological map of the Gebel El-Bakriyah area (scale 1:25000).
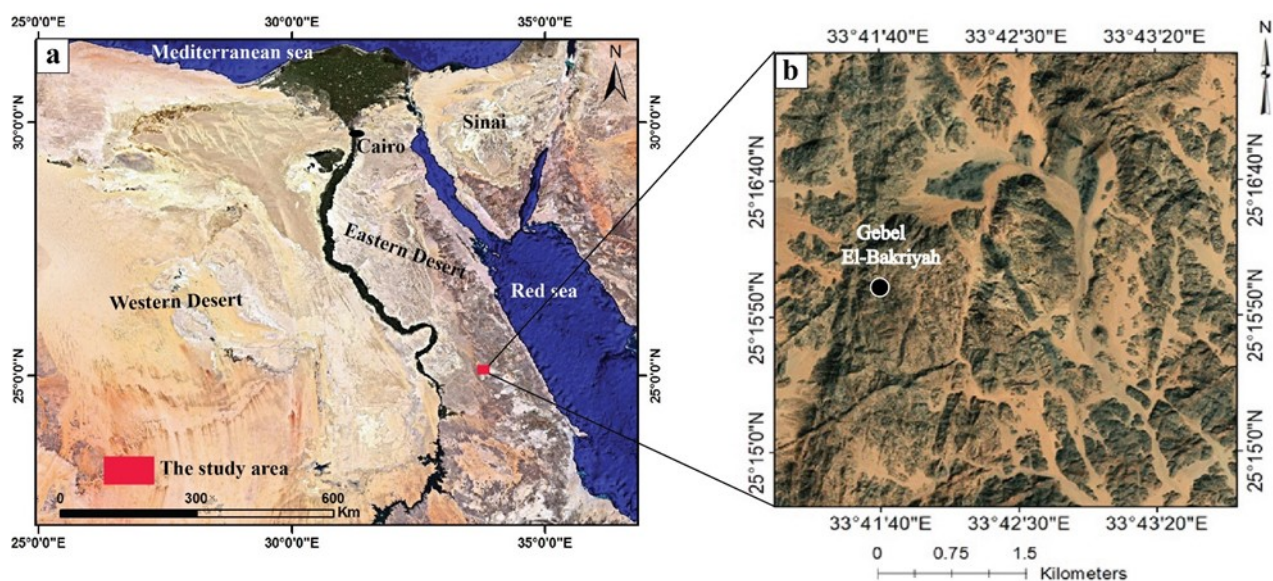

Figure 1. a) Location map of studied area, b) Satellite image subset shows Gebel El Bakriyah area.

2. Field Observations and Petrographic Characteristics

In field relationship, the Gebel El-Bakriyah pluton is treated here as a ring complex of younger granites that intrudes country rocks represented by older granitoid, younger gabbro, and pink granite. The pink granite is a younger granite rock that does not belong to the ring complex as the latter intrudes the former distinctly and has different mineralogical and geochemical signatures. The older granitoid in the studied area represent the so-called "GI" granites typical in the Neoproterozoic shield rocks, and formed in a typical arc setting [27]. Our field observations confirm the presence of granodiorite as the only variety of arc magmatism in the studied area and the entire central segment of the Eastern Desert of Egypt's Precambrian basement. The granodiorite

characterizes the oldest rock unit in the Gebel El-Bakriyah area and low- to moderate-relieved masses in the southeastern corner of the area (Figure 2). Typically, it has a medium to coarse grain size, grey color and is by apophyses of the younger granites in the form of small bosses and dykes (Figure 3a). To the north and northeast of the Gebel El-Bakriyah central felsic pluton, there are four small masses of younger gabbro studied recently by [28]. They affiliated them to the post-collisional mafic magma that was generated after the cease of magmatism in the arc from which the relatively younger granodiorite. The younger gabbro masses occur as low hills, coarse-grained, and vary in color from light gray to greenish black. The color variation is controlled by the proportions of calcic plagioclase (felsic, light color) and the ferromagnesian minerals (mafic, dark color), so occasional existence of a

melanocratic variety as "melagabbro" can be observed in spots with the minor content of calcic plagioclase. The eastern part of gabbroic rocks is invaded by several mafic and felsic dykes (Figure 3b). On a petrographic basis, three varieties of younger gabbro can be distinguished: troctolite, olivine gabbro, and hornblende gabbro. The hornblende gabbro is commonly altered and characterized by the lack of olivine, the existence of abundant hornblende, which is in turn altered to other amphibole species (tremolite-actinolite) (Figure 4a), highly kaolinized and sericitized calcic plagioclase (Figure 4b), minor biotite, and opaque minerals. The latter are represented by Fe-Ti oxides as homogeneous or intergrown magnetite and ilmenite. On the other hand, troctolite consists essentially of olivine that reaches up to ~40% of the rock volume, calcic plagioclase, few clinopyroxenes (augite), Fe-Ti oxides (magnate and ilmenite) and sulfides (pyrrhotite and pyrite). The olivine gabbro consists mainly of plagioclase and clinopyroxene, in addition to a considerable amount of olivine ($\geq$ 10%) and Fe-Ti oxides. Like the other gabbroic varieties, plagioclase in the olivine gabbro is highly altered to kaolinite (Figure 4c). By volume, the area's predominant rock unit is pink granite, which has a medium to a high degree of rough topography, is medium to coarse-grained, heavily jointed, and is often pink in color due to a high concentration of K-feldspars. Our field observations reveal the common presence of granodiorite xenoliths in the pink granite (Figure 3c). In the field, the pink granite is monotonous (Figure 3d) with no distinct variations in color or mineralogy over a distance. Microscopically, the pink granite comprises mainly potash feldspar, quartz, and biotite. The plagioclase is altered to kaolinite (Figure 4d). Accessory minerals include minor martitized magnetite, zircon, and titanite.

The Gebel El-Bakriyah ring complex comprises an alkali feldspar granite outer zone and a syenogranite inner zone (Figure 3f). The alkali feldspar granite is yellowish-brown to pink in color, highly fractured. Its relief is typically higher than the country rocks outside the semi-circular ring complex. Alkali feldspar granite is characterized by visible quartz, barite, and fluorite veins. This granite variety is characterized by being perthitic on the microscopic scale. It is made of alkali feldspars (orthoclase and sodic plagioclase), quartz, and some accessory minerals like zircon, fluorite, and magnetite. In common sense, the alkali feldspars are altered to a mixture of sericite, kaolinite, and Fe-hydroxides (Figure 4d). Occasionally, the syenogranite is non-conformably overlain by the Nubian facies sandstone that was deposited during the Cretaceous (Figure 3f). A down represents the Nubian sandstone faulted block border controlled by two essential fault planes following an NW-SE trend. The syenogranite consists of either homogeneous or perthite feldspar, quartz, biotite, and accessories (zircon, titanite, xenotime, barite, and fluorite). Figures 4e and 4f show highly altered alkali feldspars to kaolinite/Fe oxide mixtures and sericite to a lesser extent. Finally, and on a chronological aspect based on the field relationships and contacts, the Neoproterozoic shield rocks that have emerged in the Gebel El-Bakriyah area can be ordered as follows: (1) older granitoid, younger gabbros, and pink younger granite country rocks (oldest), (2) the ring complex, and (3) rhyolite, aplite, and basalt dykes and mineralized quartz veins (youngest).
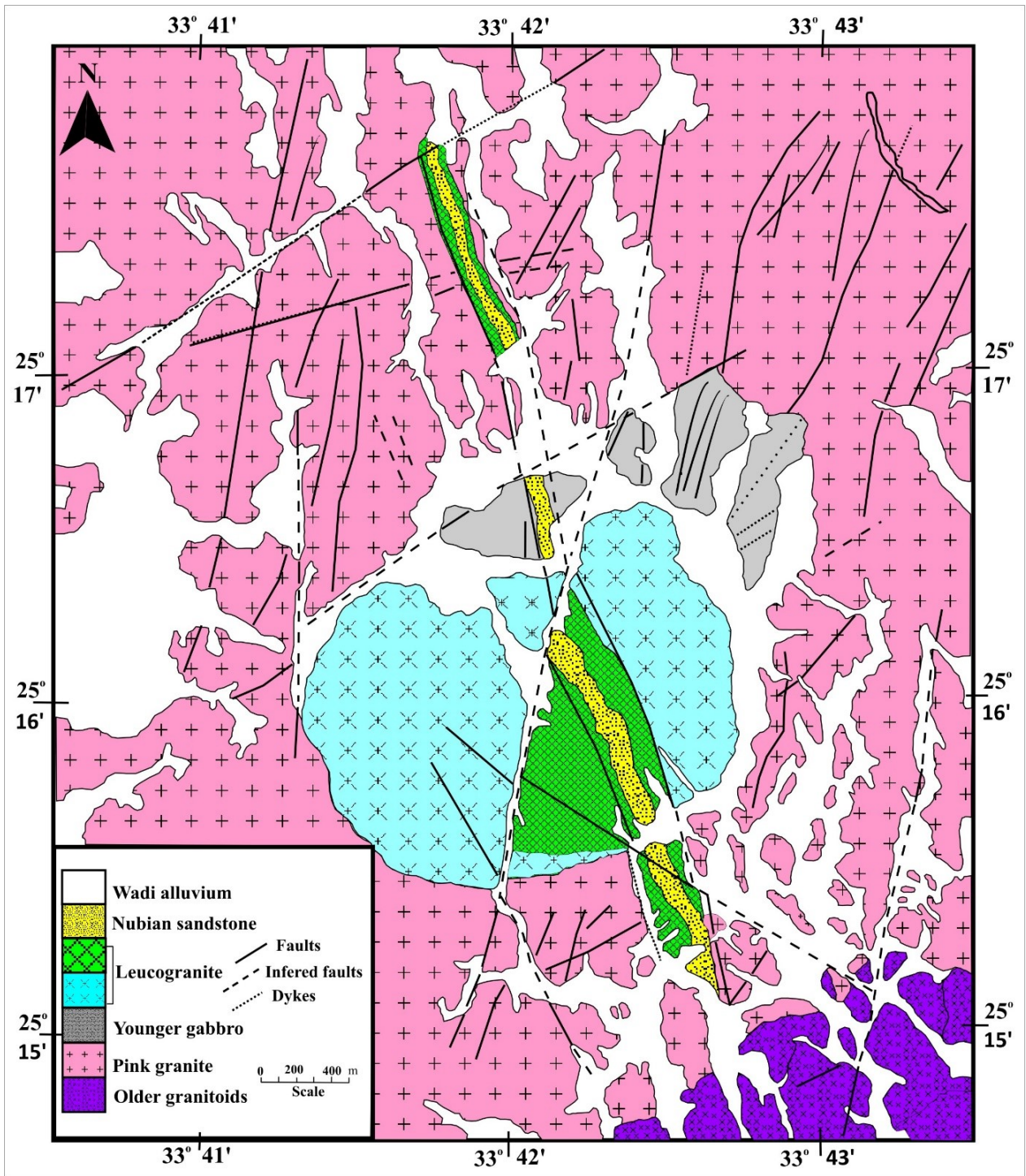
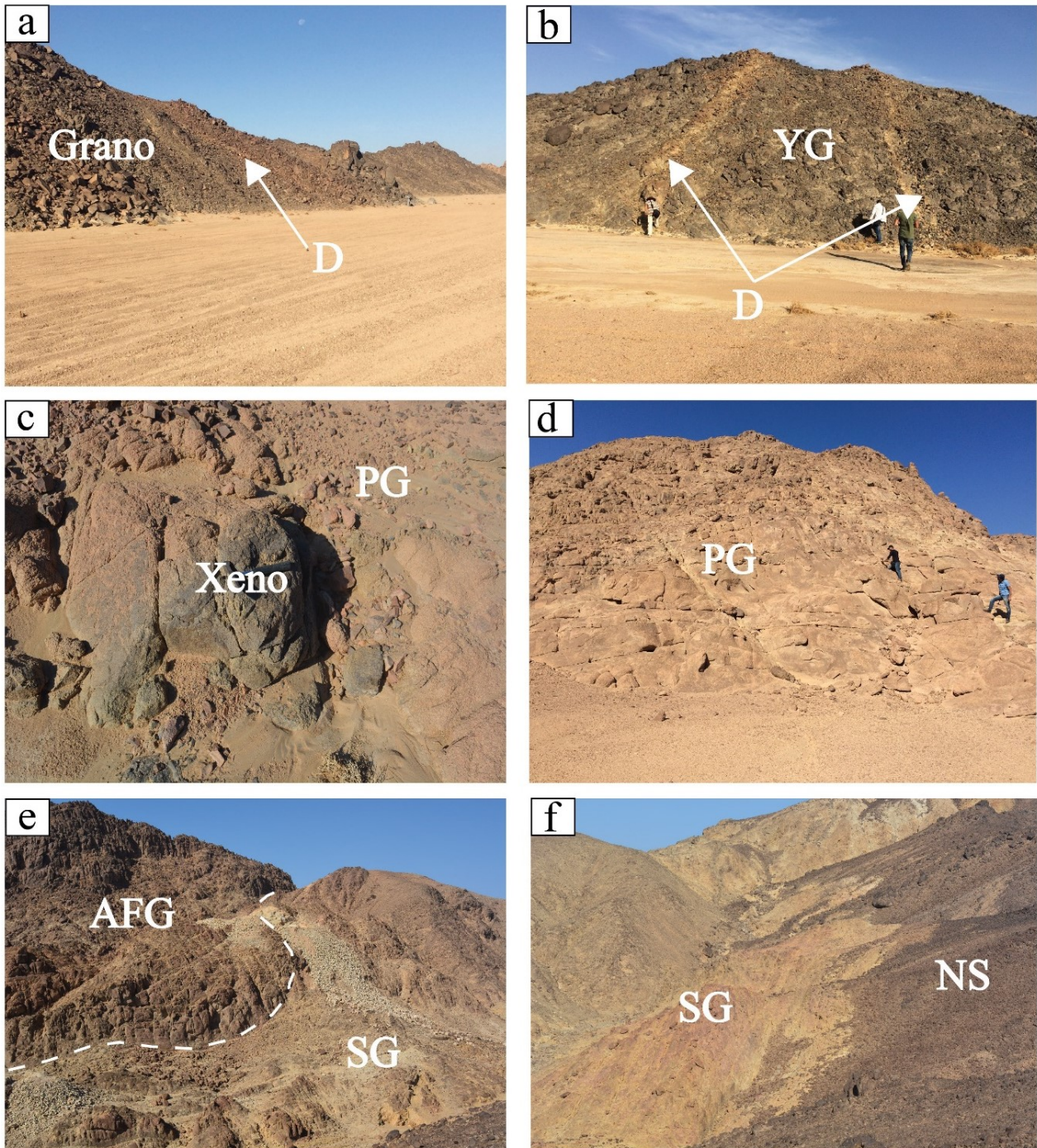**Figure 2. Geological map of Gebel El Bakriyah area from [22].**

Figure 3. Field relationships. a) Granodiorite (Grano) as the older granitoid traversed by dykes (D), b) The younger gabbros (YG) traversed by dykes (D), c) Granodiorite xenolith (Xeno) in the pink granite (PG), d) Monotonous nature of the pink granite (PG), e) Sharp contact between alkali feldspar granite (AFG, outer zone of the El-Bakriyah ring complex) and syenogranite (SG, inner zone), and f) Syenogranite (SG) capped by the Phanerozoic sediments represented by the Nubian facies sandstone (NS).
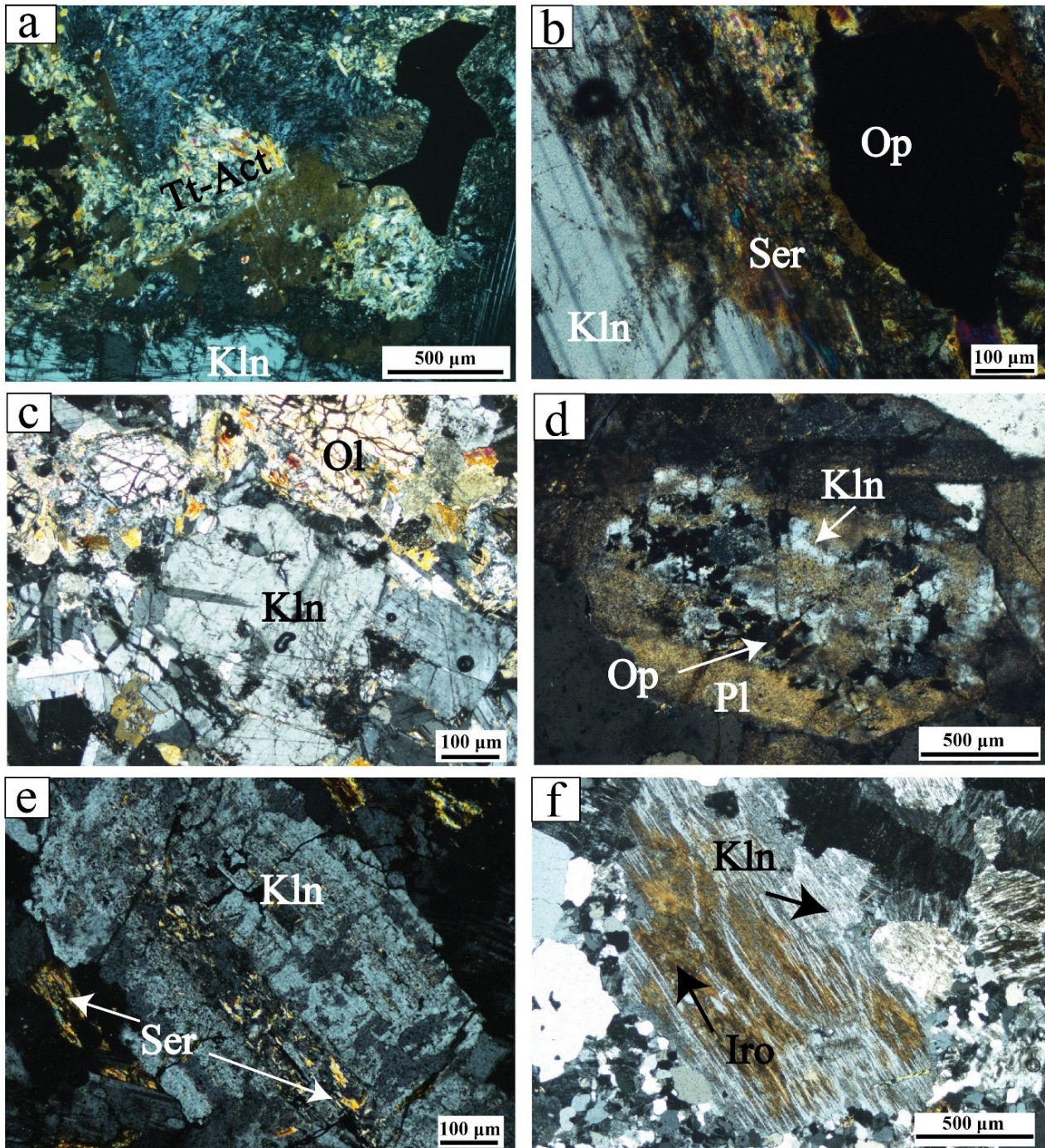
Figure 4. Alteration mineralogy of the younger gabbros and granites. All photomicrographs are taken in crossed-Nicols. a) Tremolite-actinolite aggregates (Tt-Act) and Kaolinitized plagioclase (Kln), altered hornblende gabbro, b) Sericitized (Ser) and kaolinized (Kln) calcic plagioclase juxtaposing opaques (Op), altered hornblende gabbro, c) Association of olivine (Ol) and kaolinitized plagioclase (Kln), olivine gabbro, d) Sodic plagioclase (Pl) showing extensive alteration to fine opaques (Op) and kaolinite (Kln), alkali feldspar granite, e) Extensive kaolinization (Kln) and slight sericitization (Ser) of homogeneous K-feldspar, syenogranite, and f) Alteration of perthite into kaolinite (Kln) and Fe-oxides (Iro).

3. Procedures and Techniques

Processed satellite images (Landsat-8 OLI) and spectral signature data are used to achieve lithological differentiation and mapping of the various younger granite types and younger gabbros. Figure 5 explains the techniques employed to achieve the objectives. The data used in this work can be divided into three major categories: (a) optical remote sensing data, (b) spectral data obtained in the laboratory, and (c) collateral data. Field notes and the gathering of published works are examples of the collateral data that explain the general geology and previous maps of the Gebel El-Bakriyah area. Nearly all rock units covering the studied area are sampled during fieldwork, and only 33 samples are selected for the petrographic study. In each sample, three chips were prepared in different directions. The satellite data was downloaded from the United States Geological Survey (USGS) website. Optical remote sensing data consist of the Landsat-8 OLI multispectral bands combined with Sentinel-2's high-resolution band 2 (10 m). Radiometric and geometric correction was applied to the date that was adjusted to UTM zone 36° N (WGS-84 datum) via means of the USGS/EROS center. To acquire accurate results from the sensor, radiometric calibration was performed by translating the digital digits DN to the spectrum reflectance using the ENVI 5.1 software.

In general, the image processing method's main goal is to improve the spectral properties of satellite images, which might lead to highlighting geologic features in contrast to the background. Several methods are used including band combination, false color composite, and principal component analysis. On February 11, 2013, Landsat 8 was launched on an Atlas-V 401 rocket from Vandenberg Air Force Base in California using an extended payload fairing (EPF) made by United Launch Alliance, LLC (The Landsat 8 Launch in Quotes). The Thermal Infrared (TIS) and Operational Land Imager (OLI) are the two scientific sensors of the Landsat-8 satellite (TIRS). These two sensors provide seasonal coverage of the global landmass at a spatial resolution of 30 meters (visible, NIR, SWIR), 100 m (thermal), and 15 m (panchromatic). Operational Land Imager (OLI) generates 9 spectral bands (Band 1 to 9) and is onboard Landsat-8. Thermal Infrared Sensor (TIRS) consists of 2 thermal bands with a spatial resolution of 100 m.

Rock and mineral reflection spectroscopy can provide helpful diagnostic data on their elemental and mineralogical composition [29]. The distinctive reflectance and emittance characteristics of specific features or objects are displayed in spectral signature curves, which could be used to identify fingerprints. While spectral emittance analysis reveals changes in silicate composition among primary lithologies, spectral reflectance analysis offers information on the distribution of essential minerals [30]. Similarly, spectroscopy proved its efficiency in the case of hydrothermal alteration zones in terms of their mapping and accurate localization of natural resources. To evaluate the spectral behavior of the rock units in the Gebel El-Bakriyah area, systematically collected 14 rock samples were grounded to a particle size of fewer than 250 μm using a Jasco V-770 double beam spectrometer housed at the National Research Centre, Dokki, Egypt. The spectra reflectance of powdered samples is generally more homogenous than that of rock samples. In addition, they exhibit high reflectance because of significant surface scattering and less volume scattering. In the following sections, we discuss the different methods of remote sensing to achieve the paper's primary goal. This could produce a detailed geological map of the studied area. In this respect, we follow the aspects of [31], particularly the issues of pixeling, band resolution, and enhanced reflectance. Some trials have been conducted using processed images and spectral data to map the granitic rocks of Egypt [14, 26] in the last four years.
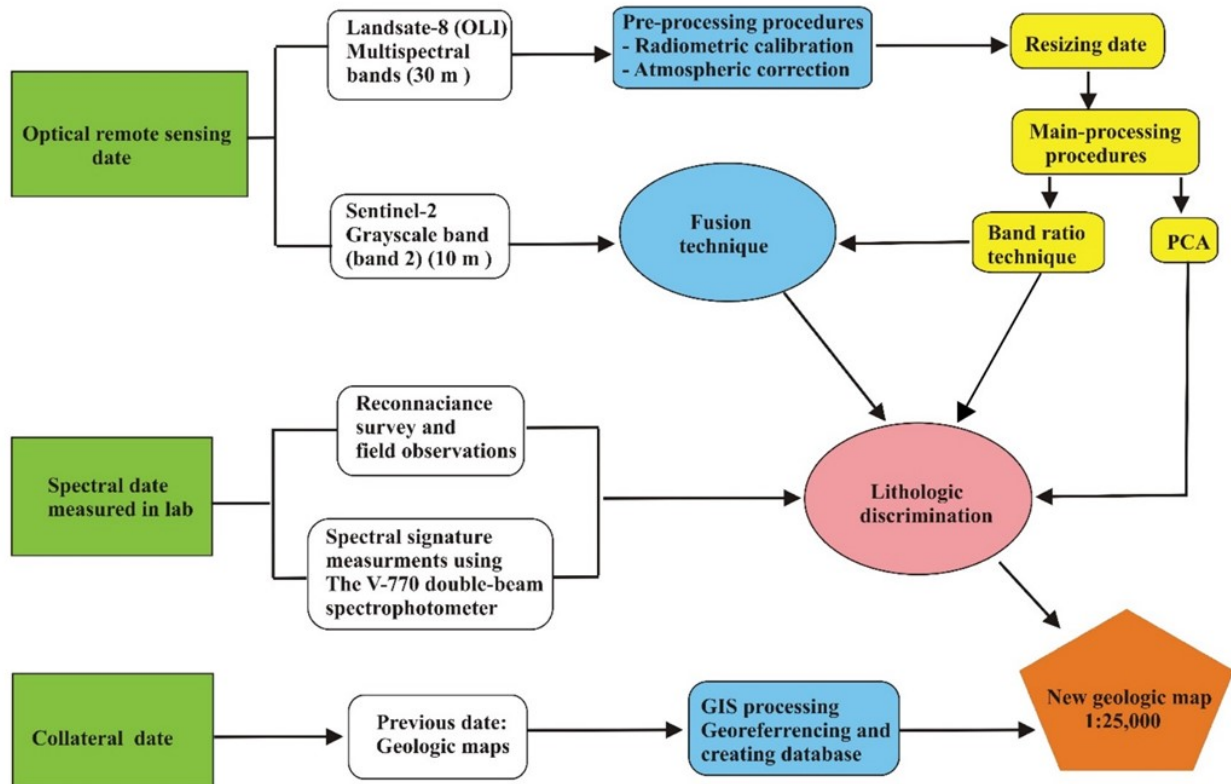
Figure 5. Remote sensing chart illustrating procedures followed in the present work.

4. Results

4.1. Spectral characteristics of Gebel El-Bakriyah plutonic rocks

In the framework of our present study, an in-depth description of spectral curves is provided. Table 1 shows the spectral and mineralogical properties of the El-Bakriyah granitic pluton types examined. Figure 6 displays the spectral profiles of El-Bakriyah granites and gabbros noted in the studied area. Figure 6a illustrates the curves of two pink granite samples' reflectance. It exhibits the following spectral features: (1) week broad absorption feature is recorded near 0.9 μm (sample# S8), (2) There are three significant absorption signatures near 1.4 m, 1.9 m, and 2.2 m wavelength areas. Figure 6b shows the reflectance profiles of three alkali feldspar granite samples. Sample # S7b displays two deep absorption characteristics at wavelengths of 1.9 and 2.2 m in addition to broad absorption features at 0.9 m. The reflectance spectral curves of three syenogranite

samples are presented in Figure 6c. Three absorption signatures distinguish them at wavelengths in the 1.4 m, 1.9 m, and 2.2 μm wavelength regions. Figure 6d shows the spectral profiles of three younger gabbro varieties (olivine gabbro, troctolite gabbro, and hornblende gabbro). The hornblende gabbro shows the lowest reflectance percentage compared with the other two gabbroic varieties. Two main absorption features are observed in all spectral curves around 1 μm and 2.2 μm. Spectra of pink granite, alkali feldspar granite, and syenogranite in ENVI (Figure 7) are characterized by an abrupt increase from band 3 to band 6, followed by a decreasing reflectance. On the other hand, the sum of younger gabbros is characterized by a sudden increase in reflectance from band 3 to band 5, followed by a final reflectance decline. All rock units have stability in reflectance from band 1 to band 3.

Table 1. Summary of mineralogical and spectral signatures of different rock varieties of post-collisional intrusive rocks at Gebel El-Bakriyah area.

| Rock unit	Mineralogy	Characteristic spectral bands
	Troctolite	
Younger gabbro	• 15-40% modal olivine • Ca-plagioclase and pyroxene • Sericitized plagioclase • Fe-Ti oxides (martitized magnetite and ilmenite) • Minor sulphides (pyrrhotite and pyrite)	• Small absorption band at 1.4 μm • Broad absorption band at 2.2 μm • Small absorption band at 2.3 μm
	Olivine gabbro	
	• ≥ 10% modal olivine • Ca-plagioclase and pyroxene • Kaolinitized plagioclase • Fe-Ti oxides (martitized magnetite and ilmenite)	• Strong broad absorption band at 1 μm • Weak broad absorption bands at 1.9 and 2.5 μm
	Hornblende gabbro	
	• No olivine • Frequent amphiboles (hornblende altering to tremolite and actinolite) • Sericitized and kaolinitized plagioclase • Fe-Ti oxides (martitized magnetite and ilmenite)	• Weak broad absorption bands at 0.7 and 1 μm • Moderate sharp absorption band at 2.2 μm • Small sharp absorption bands at 2.3 and 2.35 μm
	Pink granite	
Younger granite	• K-feldspars, albite, quartz, and biotite • Accessories: zircon and titanite • Kaolinitized plagioclase • Fe-Ti oxides (martitized magnetite and ilmenite)	• Three diagnostic broad absorption bands at 1.4, 1.9, and 2.2 μm • Sometimes weak absorption band at 0.9 μm
	Alkali feldspar granite	
	• K-feldspars (homogeneous/perthite), albite, quartz, and biotite • Accessories: zircon and fluorite • Fe-Ti oxides (martitized magnetite)	• Weak to moderate absorption bands at 1.4 and 1.9 μm • Moderate absorption band at 2.2 μm
	Syenogranite	
	• K-feldspars (orthoclase/microcline perthite), albite, quartz, and biotite • Accessories: zircon, fluorite, xenotime, and titanite • Kaolinitized perthite and plagioclase	• Small absorption bands at 1.4 μm • Moderate absorption bands at 1.9 and 2.2 μm
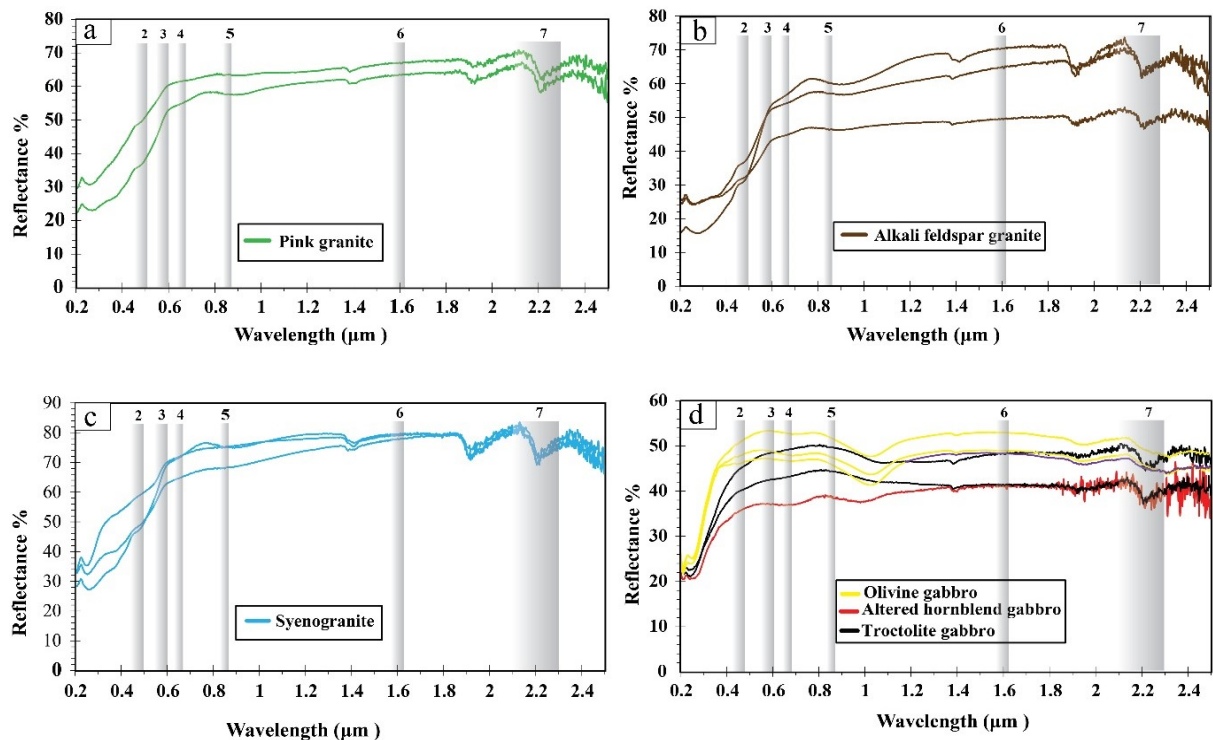
Figure 6. Spectral reflectance profiles of intrusive rocks at Gebel El-Bakariyah area. a) Pink granite, b) Alkali feldspar granite, c) Syenogranite, and d) Three varieties of younger gabbros.
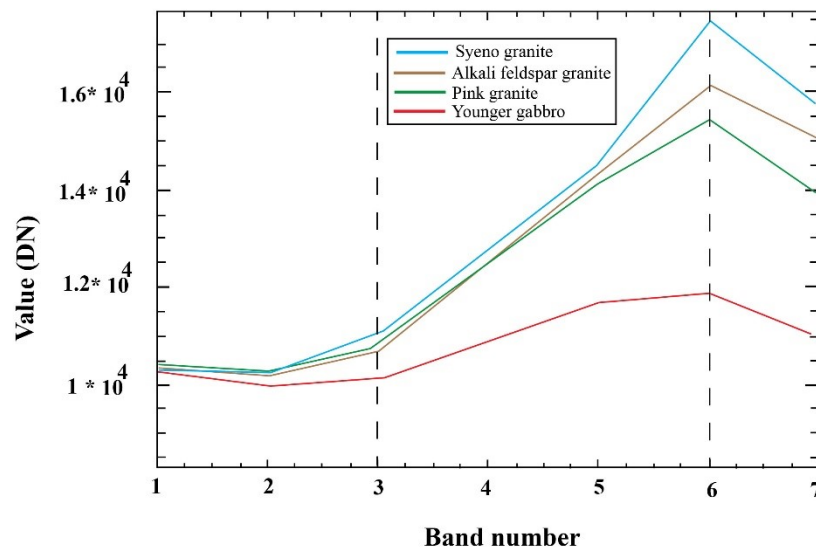
Figure 7. The reflectance spectra of younger gabbros and granites in ENVI.

4.2. Utilization in geological mapping

Principle component analyses (PCA) and band ratios are the two main image processing techniques applied throughout the present study to perform geological mapping. Figure 8 shows the results of PCA transformation images. The "PC1" is the most informative image compared to other photos, according to the Eigen-values (Table 2). It contains roughly 97.5% of an image's overall informational content. The second component, "PC2," comprises 2.1% of the original data variance, the third component, "PC3," contains 0.4%, and the fourth component, "PC4", has around 0.2%. The first component, the "PC1" image (Figure 8a), shows no discrimination between rock units and varieties but it yields accurate discrimination of Quaternary stream deposits (dark or black pixels). The second principal component, "PC2" (Figure 8b), easily discriminates the alkali feldspar granite (grey color) from the syenogranite (white color), whereas the younger gabbro has a dark grey image signature. In the "PC3| component (Figure 8c), the syenogranite is distinguished by its dark image signature, whereas the alkali feldspar granite has a whitish-grey image signature. The false color composite of PC1, PC2, and PC3 imagery is displayed in RGB in Figure 8d. It discriminates alkali feldspar granite, syenogranite, and younger gabbro by sky blue, green, and pinkish-red image signatures, respectively. The most instructive ratio for lithological discrimination of Neoproterozoic rocks in the Gebel El-Bakriyah area is the Landsat-8 band ratio gray-scale images (7/4, 6/3, 3/1). (Figures

9a, 9b, 9c). They are combined with one false color composite ratio image (7/4, 6/3, 3/1) in R, G, and B, respectively (Figure 9d), which is the most effective way to differentiate between the three types of granite and their contact. The western lobe of the pluton is lemon-green, which is indicated by alkali feldspar. The western lobe of the pluton appears lemon green in color, which indicates alkali feldspar. In the middle is a yellowish-green color that corresponds to syenogranite. Meanwhile, the eastern and western parts of the Gebel El-Bakriyah pluton are reddish-orange due to the presence of alkali feldspar granites. Outside the Gebel El-Bakriyah ring complex, pink granite is distinguishable by light blue. Dark reddish colors indicate granodiorite, blueish-black colors indicate younger gabbro, and red colors indicate Nubian facies sandstone. Figure 9 shows the results of some band ratios carried out throughout the present study. Figure 9a shows a 7/4 band ratio image in a grey scale signature. El-Bakriyah rings are easily distinguished from granodiorite rings by their white color. Figure 9b displays a 6/3 band ratio image in a grey scale signature. The younger gabbro is distinguished by its dark color and the syenogranite by its white coloration. Figure 9c shows a gray scale image with a 3/1 band ratio that readily identifies the younger gabbro with dark color. An image with a false-color composite band ratio (7/4, 6/3, 3/1) in RGB is presented in Figure 9d. It can distinguish alkali feldspar granite, syenogranite, pink granite, and younger gabbro by orange, yellow, blue, and dark blue image signatures, respectively. The fusion technique successfully improves the spatial

resolution of selected images by distinguishing and delineating different rock units. The FCC ratio image (7/4, 6/3, 3/1) is merged with band 2 of Sentinel-2. It successfully separates the three granitic varieties, namely the pink granite country rock and the two varieties of the ring complex or the El Bakriyah pluton (Figure 10). Finally, previous remote sensing tools are used to create a more detailed geologic map.

Table 2. Eigen-values of principal components (PCs) in Gebel El-Bakriyah area.

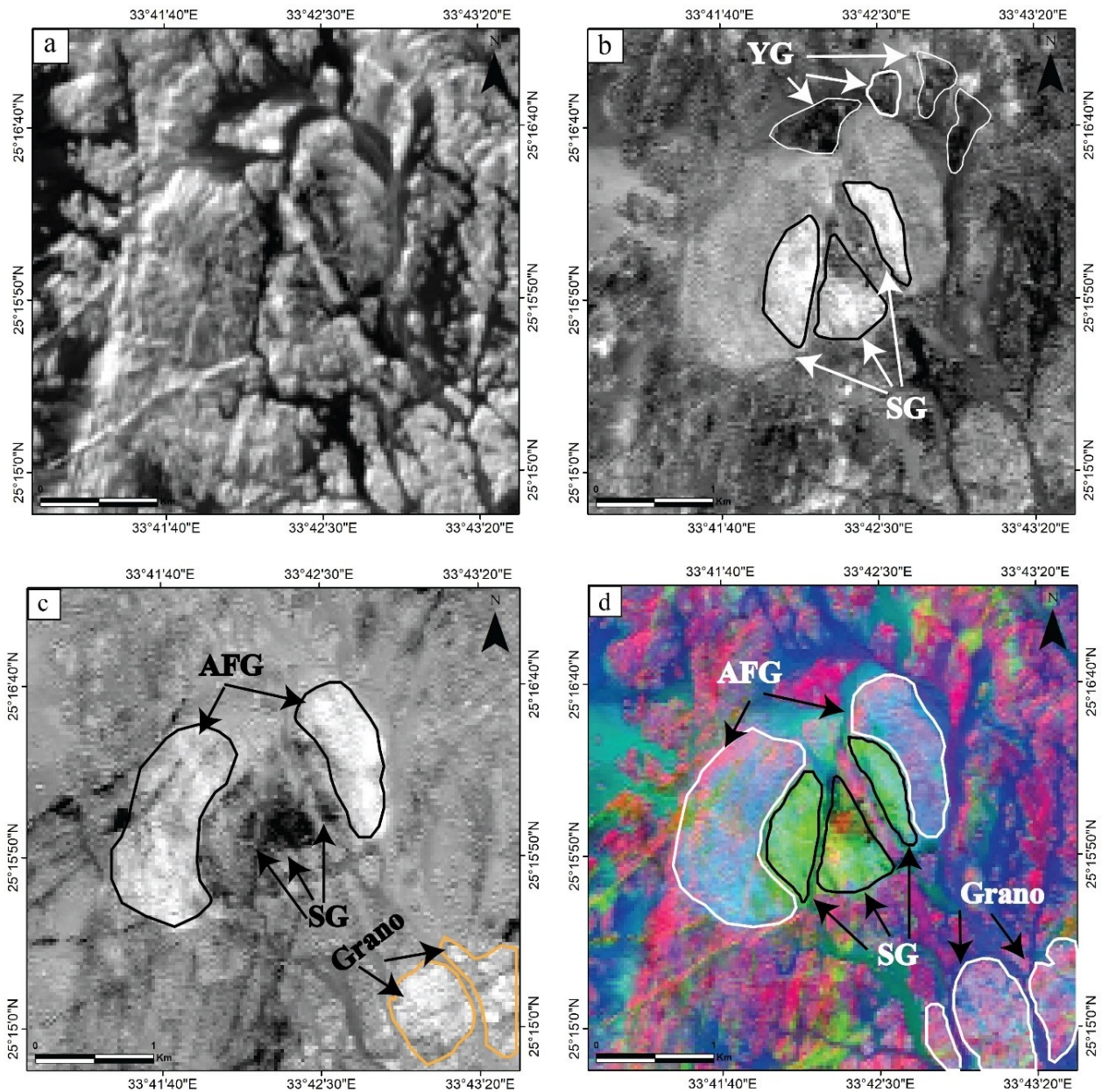| Number	Eigen-value	Percentage
PC1	22545500.29	97 %
PC2	491783.759	2.1 %
PC3	84413.07487	0.4 %
PC4	37133.82984	0.2 %
PC5	13681.07467	0.06 %
PC6	2202.077284	0.01 %

Figure 8. Processed images of the principal component analysis: PC1, PC2, PC3, and FCC shown in images from (a) to (d), respectively. The first three images are in red-green and blue (RGB). Abbreviations: Younger gabbros (YG), Granodiorite (Grano), Alkali feldspar granite (AFG), Syenogranite (SG).
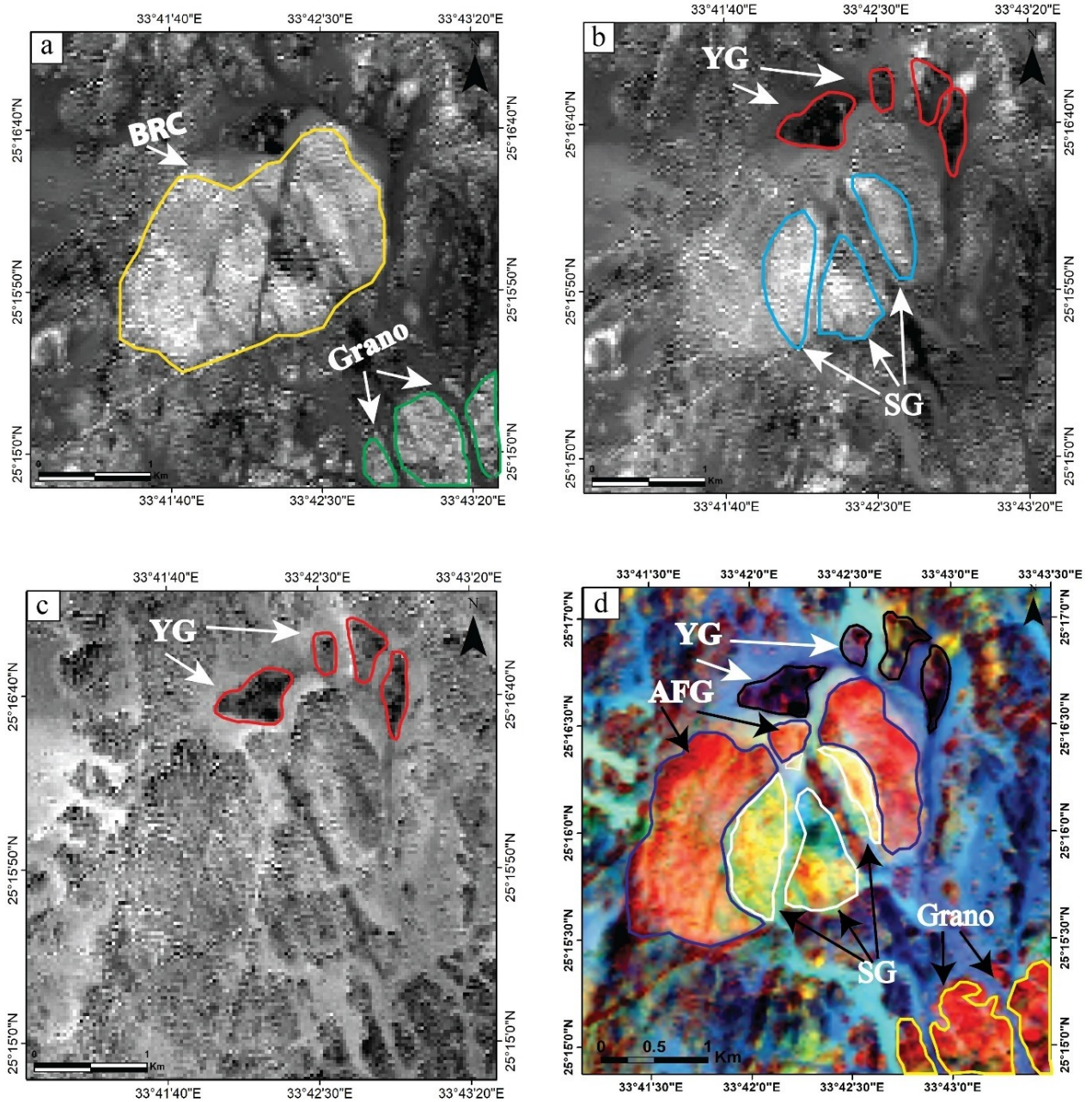
Figure 9. Band ratio images. a) 7/4, b) 6/3, c) 3/1, and d) False color composite band ratio image (7/4, 6/3, 3/1) in RGB.
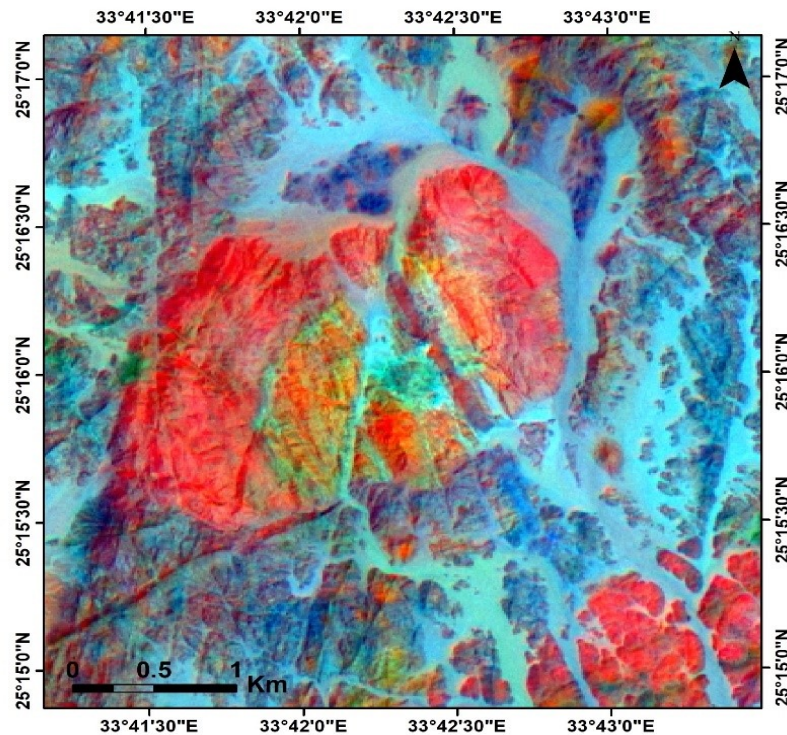
Figure 10. Fused band ratio image of Gebel El-Bakriyah ring complex, band 2 in Sentinel-2.

5. Discussion

Field visits to the Gebel El-Bakriyah area showed the existence of different varieties of plutonic rocks that are mafic to felsic from a compositional point of view. To discover the essential relationship between the spectral properties of rocks and their composition, these rocks were sampled for petrographic studies and spectral measurements. Investigation of the characterized spectral curves helped to identify the most sensitive bands for lithological discrimination, improved analysis of the spectral features of the analyzed rock units, and suggested a direct correlation between mineral composition (secondary or altered minerals) and spectral properties. Transition metals such as Fe, Mn, Cu, Ni, and Cr exhibit electronic energy level shifts in the visible and near-infrared (VNIR) range. On the other hand, the shortwave infrared (SWIR) region is defined by the spectral properties of several typical anionic constituents of minerals such as hydroxyl-bearing phases, carbonates, phosphates, and others [32]. The spectral profiles of the representative granites and gabbros are shown in Figure 11. Granite is mainly composed of tectosilicate minerals (quartz and feldspar), which have no spectral features in the VNIR and SWIR bands (0.4-2.5 μm) of the electromagnetic spectrum (EM) [29, 33], and cause a general increase in reflectance. The petrographic investigation of pink granite indicates that biotite is altered to chlorite. Hence, its spectra exhibit an apparent absorption signature near 2.35 μm, attributed to minerals containing Fe and Mg-OH such as chlorite and biotite. The alkali granites (alkali feldspar granite and syenogranite) are also subject to slight deformation, resulting in minerals such as sericite and clay. Sericitization of the syenogranite is more pronounced than in the alkali feldspar granite. Therefore, the former exhibits a sharp absorption band at 2.2 μm compared to alkali feldspar granite. Sericite has an intense Al-OH absorption feature near 2.2 μm and secondary features near 2.35 μm and 2.44 μm [34]. The alkali feldspar granite suffers from a different type of alteration (hematiztion). Thus it has a better comprehensive absorption feature at 0.9 μm than the syenogranite. Weak and broad spectral absorption bands at 0.4, 0.7, and 0.9 μm indicate Fe-bearing minerals [35]. These Fe-bearing minerals are mostly hematite and some OH-bearing phases such as Fe-oxyhydroxide. Pink granite has a lower reflectance than alkali feldspar granite and syenogranite due to mafic minerals, mostly biotite. The alkali granites (alkali feldspar granite and syenogranite) have moderate absorptions around 0.9 μm because of a moderate amount of ferric iron such as hematization. On a mineralogical basis, pink granite is a biotite

granite with a considerable amount of biotite up to ~12% of the rock volume.

This pink granite has a weak absorption feature near 2.25 µm compared with syenogranite and alkali feldspar granite, which means that they have a low amount of hydrous minerals, and consequently, they have weak OH absorption bands. Around the 2.2 µm wavelength, sharp and moderately deep absorption bands characterize syenogranite, whereas the same band is broad in alkali feldspar granite. Pink granite and syenogranite show a slight inflection near the 0.9 µm wavelength, primarily attributed to a minimal amount of ferric iron (Fe^{3+}). The alkali granites show mild spectral absorption characteristics at wavelengths of 0.7 m and 0.9 m, which is related to the ferrous ion (Fe^{+2}) predominates, such as muscovite and biotite. The absorption features near 1.4 µm and 2.2 µm areas are indicative of the presence of OH-bearing minerals, since potash feldspar and albite have been kaolinized. Alkali feldspar granite and syenogranite exhibit the hydroxyl absorption property near 1.4 µm. Remarkable kaolinization results in the 2.2 µm, 2.25 µm, and 2.35 µm bands. The characteristics of the younger gabbros spectral in El Bakriyah show variable absorption features in the short wavelength area (VNIR) around 1.0 µm as an indication of iron-bearing minerals such as pyroxene and olivine. OH-related features in the gabbros spectra near 1.42 and 2.2 µm are possibly related to either fluid inclusions or OH-bearing minerals, representing special features of clay minerals as an alteration product of plagioclase. Some spectral curves of gabbro show clear and broad absorption bands at 0.65 µm, indicating Fe-bearing minerals [35]. A broad absorption feature around 1.0 µm is typically characteristic of olivine [30]. Weak absorption bands (0.4 µm and 0.65 µm) of the pyroxene-bearing olivine gabbro reflect the presence of Fe-bearing opaque minerals (primarily magnetite and its oxidation product, martite). The spectral curve of altered hornblende gabbro has small sharp absorption features at 2.3 µm and 2.35 µm due to the presence of Fe-, Mg-hydroxide minerals, mostly amphibole minerals as secondary minerals replacing primary pyroxene. The spectral information in this discussion is used to determine the most helpful band ratio for lithological differentiation. A false-color composite image using the band ratios 7/4, 6/3, and 3/1 in R, G, and B, respectively, represents the most significant differentiation of the three granite varieties and their contact. The alkali feldspar granite, syenogranite, pink granite, and younger gabbro have orange, yellow, blue, and dark blue, respectively. The FCC ratio image (7/4, 6/3, 3/1) is fused with band 2 of Sentinel-2 to enhance well with a spatial resolution of 10 m and contributed to creating a detailed geologic map of the research region at a scale of 1:25000 (Figure 12).
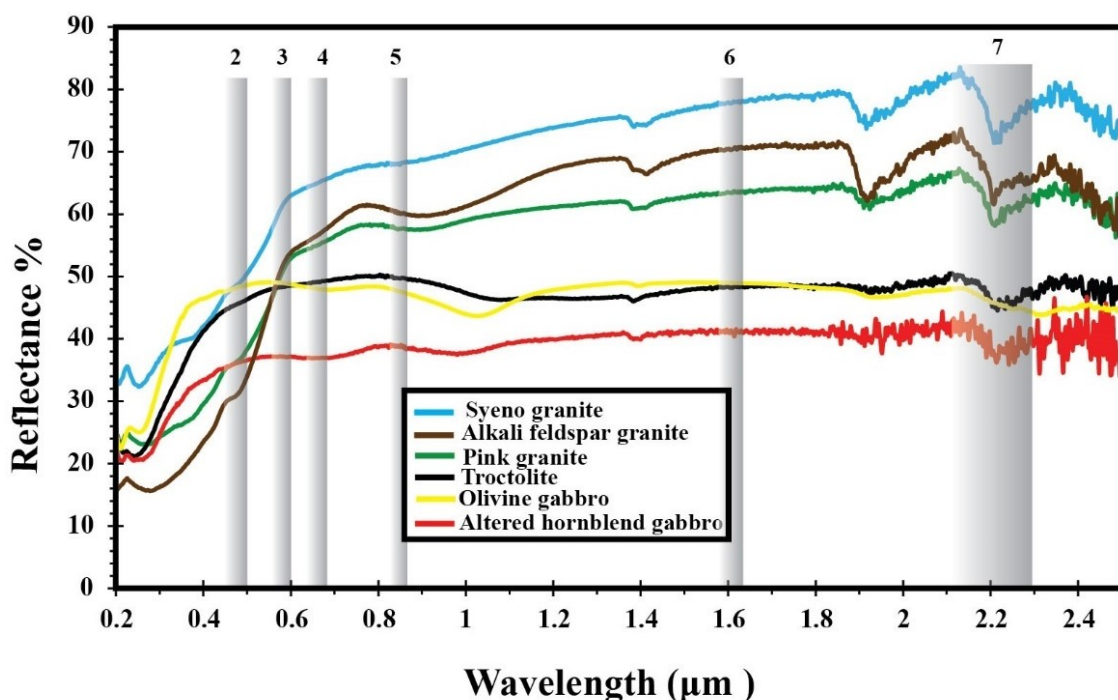

Figure 11. Collective spectral profiles of the Neoproterozoic intrusive rocks in the Gebel El-Bakriyah area.
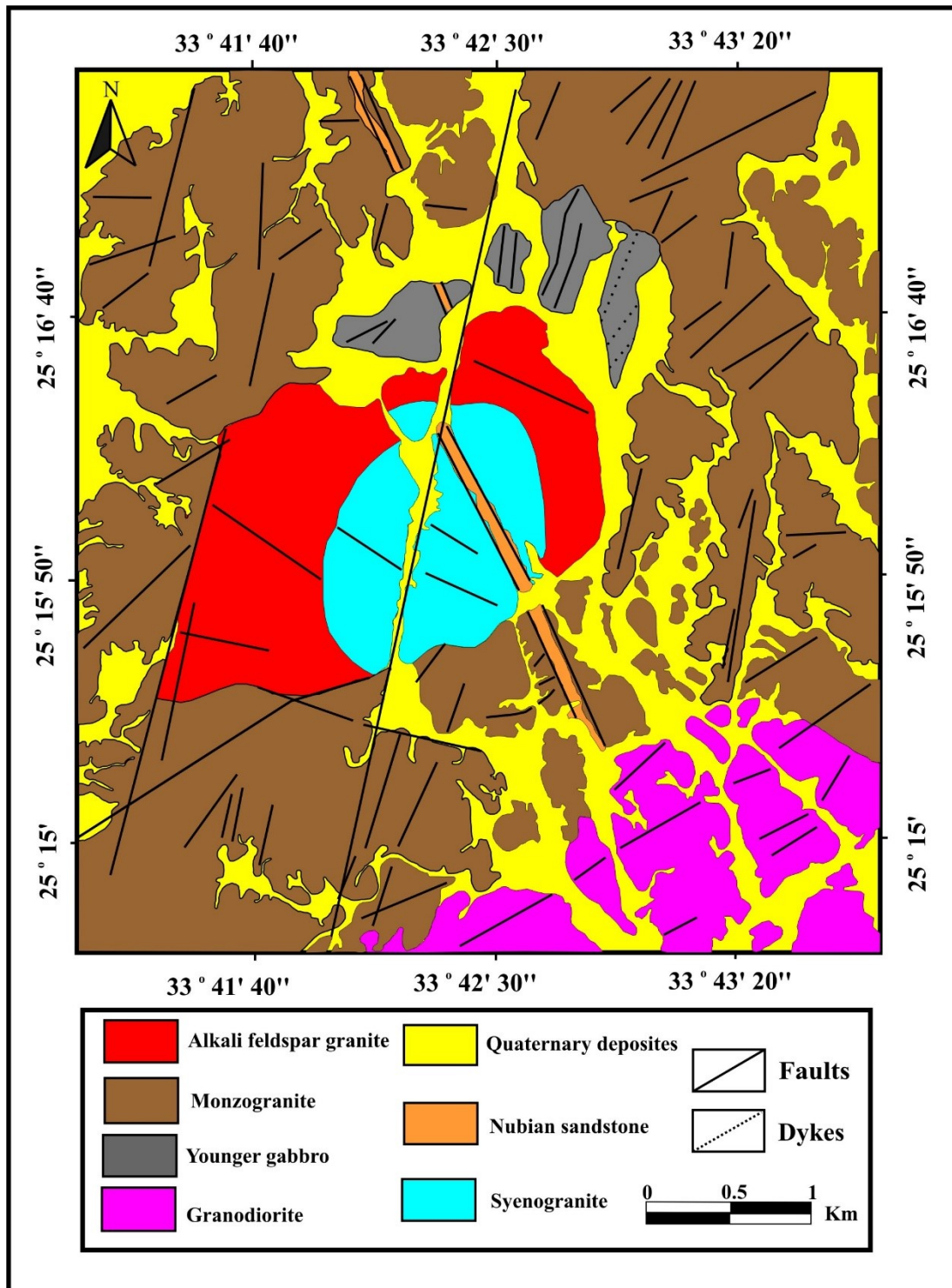
Figure 12. New geological map of Gebel El-Bakriyah area based on the integrated field, mineralogical, and spectral characteristics from the remote sensing techniques.

6. Conclusions

1) Our work contributes to the usefulness of Landsat-8 data and spectroscopy data as practical tools for geological mapping of post-collisional igneous rocks as a vital portion of the Neoproterozoic Arabian-Nubian Shield in northeast Africa and the Arabian Peninsula. Based on our results and interpretations,

combining the two tools can discriminate between lithological units of diverse chemical compositions, namely mafic (younger gabbros) and felsic (younger granites).

2) To produce a comprehensive geological map of the Gebel El-Bakriyah area, there is a need to distinguish the different rock varieties of the younger granites, either the relatively older country rocks (pink/biotite granite) or the

27

country rocks for the El-Bakriyah ring complex (alkali feldspar granite and syenogranite).

3) Field observations confirm the results for reliability, credibility, and accuracy. Therefore, we demonstrated the integration of spectroscopy reflectance and Landsat-8 images using principle component analysis (PCA), band ratios, and fusion techniques, discrimination of each lithology based on either primary mineralogy (e.g. olivine, pyroxene, biotite) or secondary mineralogy (e.g. kaolinite, sericite, martite).

4) It is worth mentioning here that the valence of some transitional metals such as iron (Fe^{2+} and/or Fe^{3+}), impacts the reflectance property of the host rock. Accordingly, the pink granite country rock and syenogranite representing the inner zone of the ring complex display a minor absorption feature around 0.9 μm, most likely owing to a slight trace of Fe^{3+}. Additionally, the alkali feldspar granite representing the outer zone of the ring complex displays a weak spectral absorption feature in the 0.7-0.9 μm wavelength region indicating the dominance of Fe^{+2} due to the presence of abundant primary micas such as muscovite and biotite. The relative abundance of primary micas also controls the strength of reflectance.

5) Similarly, the spectral reflectance of olivine gabbro is more pronounced than that of both troctolite and hornblende gabbro. In the latter, the position of the reflectance bands and their intensity are distinct due to the kaolinitization of Ca-plagioclase, and, to a lesser extent, to Oh-bearing minerals, either uralite (amphibole replacing pyroxene) or chlorite. Moreover, iron valence's effect arises because chlorite, as a secondary mineral, accommodates Fe^{2+} only in its structure.

6) Finally, the FCC ratio image (7/4, 6/3, and 3/1) merged with a high spatial resolution band 2 of Sentinel-2 using the Gram-Schmidt Pan sharpening method gives better interpretability information as the spatial resolution is improved. All our results are integrated to produce an updated geological map of the Gebel El-Bakriyah area, scale 1:25000.

Acknowledgments

References

[1]. Sultan, M., R.E. Arvidson, and N.C. Sturchio. (1986). Mapping of serpentinites in the Eastern Desert of Egypt by using Landsat thematic mapper data. Geology. 14: p. 995–999.

[2]. Kusky, T.M., and T.M. Ramadan. (2002). Structural controls on Neoproterozoic mineralization in the South Eastern Desert, Egypt: an integrated field, Landsat TM, and SIR-C/X SAR approach. Journal of African Earth Sciences. 35: p.107–121.

[3]. Madani, A.A., E.M. Abdel Rahman, K.M. Fawzy, and A. Emam. (2003). Mapping of the hydrothermal alteration zones at Haimur gold mine area, South Eastern Desert, Egypt, using remote sensing techniques. The Egyptian Journal of Remote Sensing and Space Science.6: p.47–60.

[4]. Madani, A., B. Niyazi, A. Elfakharani, and H. Osman. (2019). The Effects of Structural Elements on Groundwater of Wadi Yalamlam, Saudi Arabia using Integration of Remote Sensing and Airborne Magnetic Survey. Earth Systems and Environment. 3: p. 301–312.

[5]. Ramadan, T.M. and A. Kontny, (2004). Mineralogical and structural characterization of alteration zones detected by orbital remote sensing at Shalatein District, SE Desert, Egypt. Journal of African Earth Sciences. 40: p. 89–99.

[6]. Rowan, L.C., J.K. Crowley, R.G. Schmidt, C.M. Ager, and J.C. Mars. (2000). Mapping hydrothermally altered rocks by analyzing hyperspectral image (AVIRIS) data of forested areas in the Southeastern United States. Journal of Geochemical Exploration. 68: p. 145–166.

[7]. Rowan, L.C., R.G. Schmidt, and J.C. Mars. (2006). Distribution of hydrothermally altered rocks in the Reko Diq, Pakistan mineralized area based on spectral analysis of ASTER data. Remote Sensing of Environment. 104: p. 74–87.

[8]. Liu, F., Wu, X., H. Sun, and Y. Guo. (2007). Alteration information extraction by applying synthesis processing techniques to Landsat ETM+ data: case study of Zhaoyuan Gold Mines, Shandong Province, China. Journal of China University of Geosciences. 18: p. 72–6.

[9]. Ali-Bik, M.W., S.M. Hassan, M.A. Abou El Maaty, S.H. Abd El Rahim, S.D. Abayazeed, and W.A. Wahab, (2018). The late Neoproterozoic Pan-African low-grade metamorphic ophiolitic and island-arc assemblages at Gebel Zabara area, Central Eastern Desert, Egypt: Petrogenesis and remote sensing-based geologic mapping. Journal of African Earth Sciences. 144:p. 17–40.

[10]. Sadek, M.F., B.A. El-kalioubi, M.W. Ali-Bik, M.A.El Hefnawi, and A.A. Elnazer. (2020). Utilizing Landsat-8 and ASTER data in geologic mapping of

hyper-arid mountainous region: case of Gabal Batoga area, South Eastern Desert of Egypt. Environmental Earth Sciences. 79: p. 1–14.

[11]. Salem, S.M., NM. Soliman, T.M. Ramadan, and R.O. Greiling. (2014). Exploration of new gold occurrences in the alteration zones at the Barramiya District, Central Eastern Desert of Egypt using ASTER data and geological studies. Arabian Journal of Geosciences. 7: p. 1717–1731.

[12]. Fakhari, S., A. Jafarirad, P. Afzal, and M. Lotfi. (2019). Delineation of hydrothermal alteration zones for porphyry systems utilizing ASTER data in Jebal Barez area, SE Iran. Iranian Journal of Earth Sciences. 11: p. 80–92.

[13]. Zamyad, M., P. Afzal, M. Pourkermani, R. Nouri, , and M.R. Jafari. (2019). Determination of hydrothermal alteration zones by remote sensing methods in Tirka Area, Toroud, NE Iran. Journal of the Indian Society of Remote Sensing. 47: p. 1817–30.

[14]. Pourgholam, M.M., P. Afzal, A. Adib, K. Rahbar, and M. Gholinejad. (2022). Delineation of iron alteration zones using Spectrum-Area Fractal Model and TOPSIS decision-making method in Tarom Metallogenic Zone, NW Iran. Journal of Mining and Environment. 13 (2): p. 503–525.

[15]. Saed, S., H. Azizi, N. Daneshvar, P. Afzal, S.A. Whattam, and Y.O. Mohammad, (2022). Hydrothermal alteration mapping using ASTER data, Takab-Baneh area, NW Iran: A key for further exploration of polymetal deposits. Geocarto International - Environmental science research. 1-25. Doi/abs/10.1080/10106049.2022.2059110.

[16]. Zoheir, B. and A. Emam, (2012). Integrating geologic and satellite imagery data for high-resolution mapping and gold exploration targets in the South Eastern Desert, Egypt. Journal of African Earth Sciences. 66: p. 22–34.

[17]. Abdelaziz, R., Y. Abd El-Rahman, and S. Wilhelm. (2018). Landsat-8 data for chromite prospecting in the Logar Massif, Afghanistan. Heliyon, 4(2): p. 1–18.

[18]. Ghoneim, S.M., S.M. Salem, and M.A. El-Sharkawi. (2018). Application of remote sensing techniques on ASTER date for alteration zones extraction and lithological mapping of EL-Fawakhir–El-Sid area, central Eastern Desert, Egypt: an approach for gold exploration. Egyptian Journal of Geology. 62: p. 133–50.

[19]. Ghoneim, S.M., M.A. Yehia, S.M. Salem, and H.F. Ali. (2022). Integrating remote sensing data, GIS analysis and field studies for mapping alteration zones at Wadi Saqia area, central Eastern Desert, Egypt. The Egyptian Journal of Remote Sensing and Space Sciences. 25: p. 323–36.

[20]. Zoheir, B., A. Emam, , M. Abd El-Wahed, and N.

Soliman. (2019). Gold endowment in the evolution of the Allaqi-Heiani suture, Egypt: A synthesis of geological, structural, and space-borne imagery data. Ore Geology Reviews. 110: p. 102938.

[21]. Hamimi, Z., M. Abdelkareem, A.R. Fowler, Younis, M.H., M . Matsah, , and F. Abdalla, (2021). Remote sensing and structural studies of the Central Asir Shear Zone, Western Arabian Shield: Implications for the late Neoproterozoic EW Gondwana assembly. Journal of Asian Earth Sciences. 215: p. 104782.

[22]. Saleeb-Roufaiel, G.S., M.D. Samuel, M.E .Hilmy, and H.E. Moussa. (1982).Fluorite mineralization at El-Bakriya, Eastern Desert of Egypt, Egypt. The Journal of Geology. 26: p. 9–18.

[23]. Shirazy, A., A. Shirazi, and H. Nazerian. (2021). Application of Remote Sensing in Earth Sciences–A Review. IJSEAS-international journal of scientific engineering and applied science. 10: p. 45–51.

[24]. Calvin, WM., E.F. Littlefield, and C. Kratt. (2015). Remote sensing of geothermal-related minerals for resource exploration in Nevada. Geothermics. 53: p. 517–26.

[25]. Manuel, R., M.D.G. Brito, M. Chichorro, and C. Rosa. (2017). Remote sensing for mineral exploration in central Portugal. Minerals, 7: p. 184.

[26]. El Sobky, M.A., A.A. Madani, and A.A. Surour, (2020). Spectral characterization of the Batuga granite pluton, South Eastern Desert, Egypt: influence of lithological and mineralogical variation on ASD Terraspec data. Arabian Journal of Geosciences. 13: p. 1–15.

[27]. Johnson, P.R, A. Andresen, A.S. Collins, A.R. Fowler, H. Fritz, and W. Ghebreab. (2011). Late Cryogenian–Ediacaran history of the Arabian–Nubian Shield: a review of depositional, plutonic, structural, and tectonic events in the closing stages of the northern East African Orogen. Journal of African Earth Sciences. 61: p. 167–232.

[28]. Azer, M.K., A.A. Surour, A.A. Madani, M. Ren, and A.A.A. El-Fatah. (2022). Mineralogical and Geochemical Constraints on the Postcollisional Mafic Magmatism in the Arabian-Nubian Shield: An Example from the El-Bakriya Area, Central Eastern Desert, Egypt. The Journal of Geology. 130: p. 209–230.

[29]. Hunt, G.R. (1977). Spectral signatures of particulate minerals in the visible and near infrared. Geophysics, 42: p. 501–513.

[30]. Rowan, LC., J.C. Mars, and C.J. Simpson. (2005). Lithologic mapping of the Mordor, NT, Australia ultramafic complex by using the Advanced Spaceborne Thermal Emission and Reflection Radiometer (ASTER). Remote Sens Environ, 99: p. 105–126.

[31]. Drury, S.A.,(1987). Image interpretation in geology, p. 48.

[32]. Gupta, R.P. (2018). Spectra of Minerals and Rocks BT - Remote Sensing Geology. In: Gupta RP, editor., Berlin, Heidelberg: Springer Berlin Heidelberg. p. 23–35.

[33]. Hunt, G.R. (1980). Electromagnetic radiation: The communication link in remote sensing. Remote Sensing in Geology. p. 5–45.

[34]. Rowan, L.C. and J.C. Mars. (2003). Lithologic mapping in the Mountain Pass, California area using advanced spaceborne thermal emission and reflection radiometer (ASTER) data. Remote Sensing of Environment. 84: p. 350–66.

[35]. Clark, R.N., T.V.V. King, M. Klejwa, G.A. Swayze, and N. Vergo. (1990). High spectral resolution reflectance spectroscopy of minerals. Journal of Geophysical Research: Solid Earth. 95: p. 12653–12680.

ادغام Landsat-8 و داده‌های طیف سنجی بازتابی برای نقشه برداری از مجتمع‌های حلقه آذرین نئوپروتروزوییک پسین در یک محیط خشک: مطالعه موردی منطقه جبل البکریه، صحرای شرقی، مصر

احمد عبد الدائیم عبد الفتاح[۱]*، احمد علی مدنی[۱]، عادل عبدالله سرور[۲] و موکلس کمال آذر[۳]

۱. گروه زمین شناسی، دانشکده علوم، دانشگاه قاهره، مصر

۲. گروه علوم زمین شناسی، دانشکده علوم، دانشگاه گالالا، مصر

۳. گروه علوم زمین شناسی، مرکز تحقیقات ملی، مصر

ارسال ۲۰۲۲/۱۲/۲۶، پذیرش ۲۰۲۳/۰۱/۱۰

* نویسنده مسئول مکاتبات: aabdeldayiem@sci.cu.edu.eg

چکیده:

هدف کار حاضر افزایش استفاده از داده‌های Landsat-8 در نقشه‌برداری زمین‌شناسی زمانی است که آنها با انـدازه‌گیری‌هـای طیف‌سـنجی و مشـاهدات میدانی جفت می‌شوند. این روش برای نقشه برداری و تمایز سنگ های پلوتونیک مختلف در توده Gebel El-Bakriyah، یک جسم آذریـن عجیـب در صـحرای شـرقی مرکزی مصر به کار می‌رود. بنابراین، ما از ترکیبی از تکنیک‌های سنجش از دور مانند آنـالیز مؤلفـه‌های اصـلی (PCA)، نسبت‌های بانـد، تکنیـک همجوشـی و اندازه‌گیری‌های طیف‌سنجی برای تفسیر سنگ‌شناسی آذرین استفاده می‌کنیم و یک نقشه زمین‌شناسی جدید از منطقه Gebel El-Bakriah تهیه شـده اسـت. تصویر کامپوزیت اصلیPC1، PC2 و PC3 با رنگ قرمز، سبز و آبی (RGB) بین گرانیت فلدسپات قلیایی، سینوگرانیت و گابرو جوان‌تر تمایز داده شده است. بـه طور کلی، پروفایل‌های طیفی گرانیت‌ها را سه ویژگی جذب متمایز در مناطق طول موج ۱٫۴، ۱٫۹ و ۲٫۲ میکرومتر نشان مـی‌دهنـد. ایـن ویژگـی‌هـا عمـدتاً بـه محصولات معدنی تغییر یافته مانند کائولینیت، سریسیت و کلریت نسبت داده می‌شود. پروفایل‌های طیفی گرانیت‌های فلدسپات صورتی و قلیایی ویژگـی جـذب گسترده‌ای را در ۰٫۹ میکرومتر نشان می‌دهد که به محتوای قابل توجه آهن نسبت داده می‌شود. پروفایل‌های طیفی گابروهای تازه و جوان ویژگی‌های جذبی در حدود ۱ میکرومتر و ۲٫۲ میکرومتر را نشان می‌دهند. یک تصویر ترکیبی با رنگ کاذب، دقیق‌ترین تشخیص را از سه نوع گرانیت جوان‌تر با نسبت‌های جوان‌تر باند ۴٫۷، ۳٫۶ و ۱٫۳ در RGB ارائه می‌کند. داده‌هایی که در کار حاضر نشان داده می‌شوند، سودمندی تصاویر و اندازه‌گیری‌های طیف‌سنجی Landsat-8 را به عنوان یـک گروه‌بندی غالب برای تشخیص و نقشه‌برداری سنگ‌های سپر نئوپروتروزوییک در صحرای شرقی مصر تقویت می‌کنند.

کلمات کلیدی: مجتمع حلقه البکریه جبل، گرانیت جوان، گابرو جوان، Landsat-8/Sentinel-2، طیف سنجی.